Mechanics of Structure Genome-Based Nonlinear Shell Analysis

Yufei Long* and Wenbin Yu†
Purdue University, School of Aeronautics and Astronautics, West Lafayette, IN 47907, USA

Juan M. Fernandez‡ and Andrew C. Bergan§
NASA Langley Research Center, Hampton, VA 23666, USA

In this paper, a mechanics of structure genome (MSG)-based nonlinear shell theory is introduced. The theory uses an implicit algorithm combining the Euler's and Newton's method that can be applied for shell modeling as well as 3D homogenization. This theory has been implemented into the general-purpose constitutive modeling code SwiftComp, which was originally developed for linear analyses. For the convenience of implementing different nonlinear material models, the SwiftComp user material (SCUMAT), which has a similar interface to the Abaqus user subroutine UMAT, is developed. The capability of the MSG-based nonlinear shell is validated with numerical examples with different material models. A 2-step nonlinear homogenization, with a micromechanics step and a shell analysis step, is demonstrated.

I. Introduction

Thin-ply high strain composites (TP-HSC) are gaining more and more interest due to their low weight and high flexibility. TP-HSC are especially useful for small satellite application, in which TP-HSC are made into deployable structures that can greatly reduce the size of the satellites. However, due to the large deformation and long stowage time of these deployable structures, nonlinear behavior is observed, such as viscoelasticity, viscoplasticity, and time-dependent yielding [1–3]. Since most TP-HSC parts have a large surface area and a small thickness, they are best suited to be modeled as shells. Consequently, in order to have a better understanding of the behavior of TP-HSC deployable composites, a high-fidelity nonlinear shell model needs to be developed.

Research on the nonlinear behavior of shells has focused on different aspects. Both geometric and material nonlinearity have been discussed. Most of the studies analyze material nonlinearities, either homogeneous material or composites, with 3D solid models, and then apply on shells through the lamination theory or developing shell finite elements that use the 3D constitutive relations. Ramm and Matzenmiller [4] developed a formulation for elasto-plastic shells based on Newton's method and the concept of degenerated solid, which requires the normal stress to be zero. Swaddiwudhipong and Liu [5] analyzed the elasto-plastic response of shells using a shell element based finite element

*Graduate Research Assistant, School of Aeronautics and Astronautics, 1105 Challenger Ave 100, West Lafayette, IN 47907.
†Professor, School of Aeronautics and Astronautics, 701 W. Stadium Avenue West Lafayette, IN 47907, and AIAA Associate Fellow.
‡Research Aerospace Engineer, Structural Dynamics Branch, AIAA Senior Member.
§Research Aerospace Engineer, Durability, Damage Tolerance, and Reliability Branch, AIAA Member.

approach with a time marching scheme. Wang et al. [6] developed an elastic-viscoplastic model for composites and implemented it through plate/shell finite elements based on lamination theory. Peng and Cao [7] studied the nonlinear elastic behavior of textile composites using a 2-step homogenization method. Both steps are based on 3D solid models, where the effective shell properties are obtained through matching the reaction force and displacement of a shell element to the representative volume element (RVE). Chen et al. [8] developed an analytical approach for heterogeneous spherical nonlinear elastic shells. Rabczuk et al. [9] developed a meshfree shell theory that can model various nonlinear shell behaviors. This model is especially suitable for crack analysis. Caseiro et al. [10] developed the formula of a shell element for nonlinear shell analysis that calculates the strain using a new set of calculating points instead of the conventional integration points. Goncalves et al. [11] analyzed the buckling and post buckling behavior of sandwich shells using a multiscale nonlinear shell theory based on the RVE analysis and first-order shear deformation theory. Currently, the number of studies on directly using nonlinear shell modeling to analyze shell behavior with material nonlinearities are limited. Development of a nonlinear shell homogenization algorithm that can be applied with various material constitutive models is critical to analyze the permanent deformation and other nonlinear behavior in TP-HSC deployable structures.

The mechanics of structure genome (MSG) [12, 13] provides a feasible solution with high efficiency and accuracy for analyzing the nonlinear behavior of TP-HSC. The MSG is a general theory that unifies micromechanics and structure analysis. MSG-based analysis is based on the structure gene (SG), defined as the smallest mathematical building block of the structure. It can be used for homogenization that calculates the effective properties of a structure, or dehomogenization that calculates the local fields based on structural analysis results. MSG-based plate and shell models have been developed for different kind of problems [14–16]. However, since MSG was originally developed for linear analyses, modification of the original MSG formulation is necessary for applying it to nonlinear analyses. The variational asymptotic method (VAM) [17], the mathematical method MSG is based on, has been applied to analyze nonlinear beam [18, 19] and micromechanics [20, 21] problems, however a general-purpose shell model has not been developed.

In this paper, the kinematics of MSG-based shell theory is introduced first, followed by the formulation of the nonlinear shell model. The solving algorithm of the nonlinear shell model is based on an Euler-Newton combined method. At the beginning of each increment an Euler step is carried out to proceed the loading in the tangential direction, and then a Newton step is carried out to ensure the convergence of the increment. The shell model presented is generalized and implemented into a nonlinear version of SwiftComp, an MSG-based homogenization tool. A workflow of nonlinear shell analysis is proposed, with this paper focusing on the constitutive modeling for shells for providing nonlinear shell properties to the structural analysis. A 2-step homogenization for modeling laminates and woven composites is introduced. For the convenience of implementing various nonlinear material models for the shell, a user material interface SCUMAT is also developed for SwiftComp. Several constitutive models were implemented into SCUMATs and tested with numerical case studies.

II. Kinematics

The mechanics of structure genome (MSG) formulation starts with kinematics that relates the 3D kinematic fields of the original structure to those of the macroscopic model and fluctuating functions. For this purpose, two sets of coordinate systems are introduced. First are the macro coordinates x_i, which represent the coordinates of the global structure. For plates/shells only x_α describing the reference surface exist and x_3 is eliminated. Greek indices assume 1, 2, and Latin indices assume 1, 2, 3. Repeated indices indicate summation over their range unless underlined or explicitly described. Because SG is defined as the smallest building block of a structure, its size is much smaller than the deformation wavelength of the global structure, so a second set of coordinates, micro coordinates y_i, can be introduced. The macro coordinates and micro coordinates can be related with a small parameter ε, so that $y_i = x_i/\varepsilon$, but notice that ε is only used for order analysis and no specific value is needed for this small parameter. Depending on the dimension of SG, some of the y_i coordinates can be eliminated. For example, only y_3 exists for a 1D SG. Based on this coordinate system, a field function f of the original structure can be written as a function of x_i and y_i, and its partial derivative can be expressed as [22]

$$\frac{\partial f\left(x_k, y_j\right)}{\partial x_i} = \left.\frac{\partial f\left(x_k, y_j\right)}{\partial x_i}\right|_{y_j=\text{const}} + \frac{1}{\varepsilon}\left.\frac{\partial f\left(x_k, y_j\right)}{\partial y_i}\right|_{x_k=\text{const}} \equiv f_{,i} + \frac{1}{\varepsilon} f_{|i} \tag{1}$$

Here the equation is for the case of plate/shell structures with 3D SG. The corresponding equation for 2D or 1D SG can be obtained by eliminating corresponding micro coordinates similarly to linear MSG-based modeling [12, 13].

The position vector of a point in a shell can be determined by its coordinates x_i, as shown in Fig. 1, where x_α are two orthogonal coordinates in the reference surface and x_3 is the normal coordinate. Based on the concept of MSG, micro coordinate $y_3 = x_3/\varepsilon$ can be introduced. Denoting the normal vector of the reference surface as $\mathbf{b}_3$, which is also the base vector of coordinate x_3, and the position vector of a point on the reference surface as $\mathbf{r}$, the position vector of any material point in the plate/shell $\hat{\mathbf{r}}$ can be expressed as

$$\hat{\mathbf{r}}\left(x_1, x_2, y_3\right) = \mathbf{r}\left(x_1, x_2\right) + \varepsilon y_3 \mathbf{b}_3 \tag{2}$$

The vector $\mathbf{r}$ represents the intersection point between the reference surface and the normal line on which the described point is located. When taking the middle surface as the reference surface, performing average on both sides of Eq. (2) gives

$$\langle\langle \hat{\mathbf{r}}\left(x_1, x_2, y_3\right)\rangle\rangle = \mathbf{r}\left(x_1, x_2\right) \tag{3}$$

where $\langle\langle\ \rangle\rangle$ indicates average over the SG. This implies that $\mathbf{r}$ represents the through-the-thickness average of $\hat{\mathbf{r}}$.

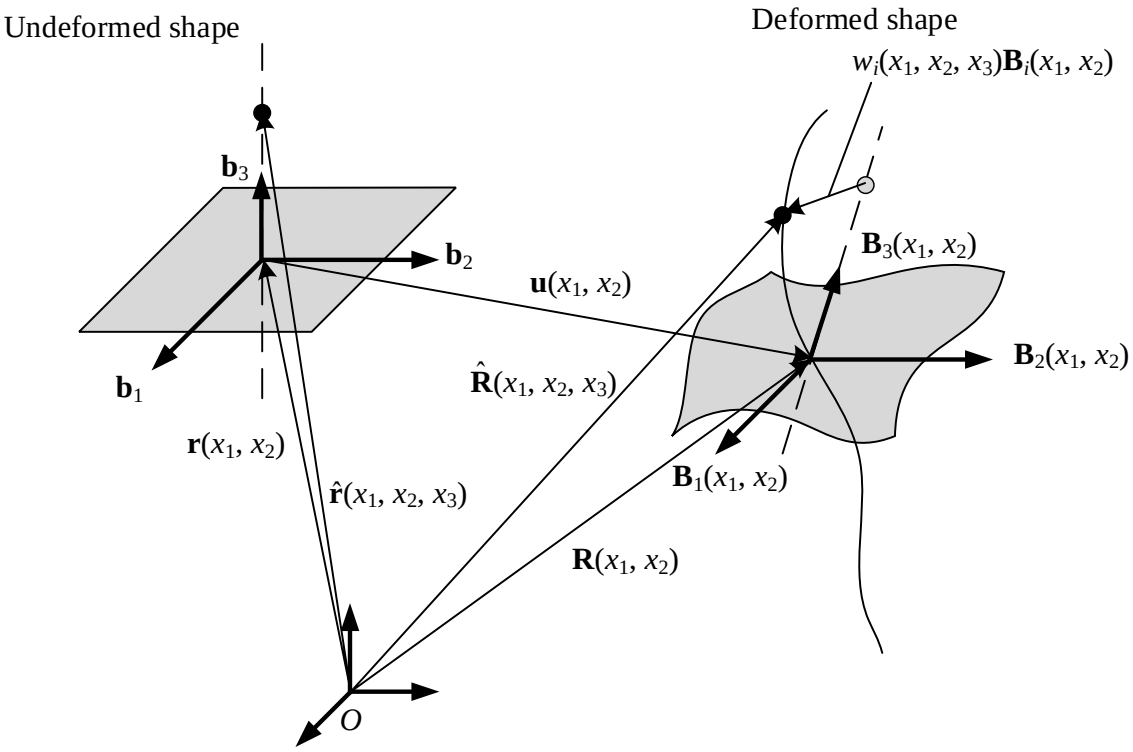

Fig. 1 Schematic of shell deformation.

The base vectors of coordinate x_α are defined as the tangent vectors

$$\mathbf{a}_\alpha\,(x_1, x_2) = \mathbf{r}_{,\alpha} \tag{4}$$

Then, Lamé parameters of the reference surface can be obtained as

$$A_\alpha\,(x_1, x_2) = \sqrt{\mathbf{a}_{\underline{\alpha}} \cdot \mathbf{a}_{\underline{\alpha}}} \tag{5}$$

These parameters can be interpreted as distance measurements on the corresponding directions of the surface. Using A_α, unit vectors in the tangential direction can be introduced as

$$\mathbf{b}_\alpha = \frac{\mathbf{a}_{\underline{\alpha}}}{A_{\underline{\alpha}}} \tag{6}$$

$\mathbf{b}_i$ form an orthonormal triad, satisfying

$$\mathbf{b}_3 = \mathbf{b}_1 \times \mathbf{b}_2 = \frac{\mathbf{a}_1 \times \mathbf{a}_2}{|\mathbf{a}_1 \times \mathbf{a}_2|} \tag{7}$$

Due to the complexity of modeling a nonlinear shell, only the classical model is considered. As a result, terms related to initial curvatures can be dropped from the governing functional to be minimized later [23], and thus the kinematics presented here is simplified accordingly.

When deformation happens, the material point described by vector $\hat{\mathbf{r}}$ in the undeformed state will have the position vector $\hat{\mathbf{R}}$ in the deformed state. Every material point in the undeformed state will uniquely have a deformation-determined position vector in the deformed state. Similar to the undeformed state, the orthonormal vector triad for the deformed state $\mathbf{B}_i$ is introduced. The relation between $\mathbf{b}_i$ and $\mathbf{B}_i$ is described using the direction cosine matrix $C\left(x_1, x_2\right)$

$$\begin{aligned} \mathbf{B}_i &= C_{ij}\mathbf{b}_j \\ C_{ij} &= \mathbf{B}_i \cdot \mathbf{b}_j \end{aligned} \tag{8}$$

so that $\mathbf{B}_i$ and $\mathbf{b}_i$ are identical when the plate/shell is undeformed. However, after rotation, $\mathbf{B}_\alpha$ are not necessarily tangential to the deformed plate/shell reference surface. For a general SG, in addition to y_3, micro coordinates $y_\alpha = x_\alpha/\varepsilon$ can also be introduced. Similar to Eq. (2), expanding $\hat{\mathbf{R}}$ based on $\mathbf{B}_i$ gives

$$\hat{\mathbf{R}}\left(x_\alpha, y_i\right) = \mathbf{R}\left(x_\alpha\right) + \varepsilon y_3 \mathbf{B}_3\left(x_\alpha\right) + \varepsilon w_i\left(x_\alpha, y_i\right)\mathbf{B}_i\left(x_\alpha\right) \tag{9}$$

where w_i are fluctuating functions to ensure Eq. (9) is able to describe all possible deformation. No assumption is made on the shape of the fluctuating functions and their exact expression will be solved later. Unlike $\mathbf{b}_i$, $\mathbf{B}_i$ is not clearly defined due to the arbitrariness of the rotation, so Eq. (9) is not unique for every point unless six more constraints are introduced. For the first three constraints, it would be convenient to set $\mathbf{R}$ to be the average of $\hat{\mathbf{R}}$ over the SG, which means

$$\left\langle\left\langle\hat{\mathbf{R}}\right\rangle\right\rangle = \mathbf{R} \tag{10}$$

In this way, the constraints should be

$$\left\langle\left\langle w_i\left(x_\alpha, y_i\right)\right\rangle\right\rangle = 0 \tag{11}$$

Before introducing the other three constraints, strains should be defined first. For small local rotations, the 3D Jauman-Biot-Cauchy strain components in the undeformed state Γ_{ij} can be written as

$$\Gamma_{ij} = \frac{1}{2}(F_{ij} + F_{ji}) - \delta_{ij} \tag{12}$$

where δ_{ij} is the Kronecker symbol, F_{ij} is the component of the deformation gradient tensor such that

$$F_{ij} = \mathbf{B}_i \cdot \frac{\partial \hat{\mathbf{R}}}{\partial x_j} \tag{13}$$

For expressing 3D strain field in terms of 2D strains, one can define 2D generalized strains as [12, 24]

$$\mathbf{R}_{,\alpha} = A_{\underline{\alpha}} \left(\mathbf{B}_{\underline{\alpha}} + \varepsilon_{\underline{\alpha}\beta} \mathbf{B}_{\beta} \right) \tag{14}$$

$$\mathbf{B}_{3,\alpha} = A_{\underline{\alpha}} \kappa_{\underline{\alpha}\beta} \mathbf{B}_{\beta} \tag{15}$$

$$\mathbf{B}_{\alpha,\beta} = A_{\underline{\beta}} \left[-\kappa_{\underline{\beta}2} \mathbf{B}_1 + \kappa_{\underline{\beta}1} \mathbf{B}_2 + \kappa_{\underline{\beta}3} \mathbf{B}_3 \right] \times \mathbf{B}_{\alpha} \tag{16}$$

where $\varepsilon_{\alpha\beta}$ and $\kappa_{\alpha\beta}$ are the 2D generalized membrane strains and curvatures. Although components $\kappa_{\alpha 3}$ appears in Eq. (16), they will not appear in the expression of 3D strains as long as local fluctuating functions are small. From Eq. (14), three more constraints can be introduced. The first two limit the direction of vector $\mathbf{B}_3$, so that it is normal to the deformed reference surface

$$\frac{\mathbf{R}_{,\underline{\alpha}} \cdot \mathbf{B}_3}{A_{\underline{\alpha}}} = 0 \tag{17}$$

It should be noted that these two constraints do not mean that the transverse shear deformation is zero. Instead, transverse shear deformation will be captured by the fluctuating functions. The last constraint can be introduced as

$$\frac{\mathbf{B}_1 \cdot \mathbf{R}_{,2}}{A_2} = \frac{\mathbf{B}_2 \cdot \mathbf{R}_{,1}}{A_1} \tag{18}$$

which implies $\varepsilon_{12} = \varepsilon_{21}$.

For the classical shell model, leading terms of the 3D strain field can be obtained using Eq. (12) – (16), so that 3D strain fields can be expressed in terms of 2D strains and fluctuating functions. In a matrix form, it is

$$\Gamma = \Gamma_h w + \Gamma_\epsilon \epsilon \tag{19}$$

where

$$\Gamma = \begin{bmatrix} \Gamma_{11} & \Gamma_{22} & \Gamma_{33} & 2\Gamma_{23} & 2\Gamma_{13} & 2\Gamma_{12} \end{bmatrix}^{\mathrm{T}} \tag{20}$$

$$w = \begin{bmatrix} w_1 & w_2 & w_3 \end{bmatrix}^{\mathrm{T}} \tag{21}$$

$$\epsilon = \begin{bmatrix} \varepsilon_{11} & \varepsilon_{22} & 2\varepsilon_{12} & \kappa_{11} & \kappa_{22} & \kappa_{12} + \kappa_{21} \end{bmatrix}^{\mathrm{T}} \tag{22}$$

Γ_h is an operator matrix for calculating derivatives with respect to micro coordinates. Terms of this matrix depend on

the dimension of the SG. For a 1D SG representing laminates, it is

$$\Gamma_h = \begin{bmatrix} 0 & 0 & 0 \\ 0 & 0 & 0 \\ 0 & 0 & \frac{\partial}{\partial y_3} \\ 0 & \frac{\partial}{\partial y_3} & 0 \\ \frac{\partial}{\partial y_3} & 0 & 0 \\ 0 & 0 & 0 \end{bmatrix} \tag{23}$$

Γ_ϵ is an operator matrix associated with 2D strains and curvatures

$$\Gamma_\epsilon = \begin{bmatrix} 1 & 0 & 0 & x_3 & 0 & 0 \\ 0 & 1 & 0 & 0 & x_3 & 0 \\ 0 & 0 & 0 & 0 & 0 & 0 \\ 0 & 0 & 0 & 0 & 0 & 0 \\ 0 & 0 & 0 & 0 & 0 & 0 \\ 0 & 0 & 1 & 0 & 0 & x_3 \end{bmatrix} \tag{24}$$

This concludes the formulation for the kinematics part of the MSG-based shell model.

III. MSG-Based Nonlinear Plate/Shell Model

A nonlinear homogenization algorithm was developed for applying the MSG-based shell model to nonlinear analysis. The MSG-based shell model is compatible with geometric nonlinearity as the kinematics in Section II is geometrically exact. For material nonlinearity, appropriate material constitutive models should be used along with the homogenization approach to be presented. For demonstrative purpose, the following derivation is based on 1D SG.

Define a state function $\mathcal{W}$ as

$$\mathcal{W}\left(\dot{\Gamma}_{ij}\right) = \frac{1}{2}\dot{\Gamma}_{ij}C^{alg}_{ijkl}\dot{\Gamma}_{kl} \tag{25}$$

where C^{alg}_{ijkl} is the tangent stiffness obtained from the material model. Then, the variational statement of this problem can be described as: among all the admissible strain rates, the actual strain rates should minimize the functional

$$U = \langle \mathcal{W} \rangle \tag{26}$$

so that

$$\delta U = \langle \delta \mathcal{W} \rangle = \left\langle \frac{\partial \mathcal{W}}{\partial \dot{\Gamma}_{ij}} \delta \dot{\Gamma}_{ij} \right\rangle = \left\langle \dot{\sigma}_{ij} \delta \dot{\Gamma}_{ij} \right\rangle = 0 \tag{27}$$

in which only the fluctuating functions are varied, and subjected to the constraints in Eq. (11). To solve the problem, the 1D SG is discretized into finite elements, so that the fluctuating functions can be expressed as

$$w\left(x_\alpha, y_3\right) = S\left(y_3\right) V\left(x_\alpha\right) \tag{28}$$

The Newton's method can be applied to solve the problem with 2D strain ε been held fixed and V being the variable. However, using the Newton's method directly may result in convergence difficulty, especially when the initial point is far from the solution. To overcome this, an Euler prediction step can be added prior to the Newton step, which means the loading process proceeds first in the tangent direction of the loading path, and then corrected to obtain the solution. The Euler step obtains the increments of 3D variables at the beginning of the current loading increment, so that the following Newton step can have a better convergence to the final solution. Substituting Eq. (19) and (28) into Eq. (26) gives

$$U = \frac{1}{2}\left(\dot{V}^{\mathrm{T}} E \dot{V} + 2\dot{V}^{\mathrm{T}} D_{h\epsilon} \dot{\epsilon} + \dot{\epsilon}^{\mathrm{T}} D_{\epsilon\epsilon} \dot{\epsilon}\right) \tag{29}$$

where

$$\begin{aligned} E &= \left\langle \left(\Gamma_h S\right)^{\mathrm{T}} D \left(\Gamma_h S\right) \right\rangle \\ D_{h\epsilon} &= \left\langle \left(\Gamma_h S\right)^{\mathrm{T}} D \Gamma_\epsilon \right\rangle \\ D_{\epsilon\epsilon} &= \left\langle \Gamma_\epsilon^{\mathrm{T}} D \Gamma_\epsilon \right\rangle \end{aligned} \tag{30}$$

with D being the 6×6 matrix form of the tangent stiffness C_{ijkl}^{alg}. Minimizing U in Eq. (29) gives

$$\dot{V} = \hat{V}_0 \dot{\epsilon} \tag{31}$$

The rate of 3D strain field can be recovered using Eq. (31) as

$$\dot{\Gamma} = \Gamma_\epsilon \dot{\epsilon} + \Gamma_h S \hat{V}_0 \dot{\epsilon} \tag{32}$$

Written in an incremental form gives

$$\Delta\Gamma = \Gamma_\epsilon \Delta\epsilon + \Gamma_h S \hat{V}_0 \Delta\epsilon \tag{33}$$

Substituting Eq. (31) back into Eq. (29) gives

$$U = \frac{1}{2}\dot{\epsilon}^{\mathrm{T}}\left(\hat{V}_0^{\mathrm{T}} D_{h\epsilon} + D_{\epsilon\epsilon}\right)\dot{\epsilon} = \frac{1}{2}\dot{\epsilon}^{\mathrm{T}} A \dot{\epsilon} \tag{34}$$

where A is the current effective tangent stiffness matrix of the shell model. By definition, the sectional force and moment N can be calculated as

$$\dot{N} = \frac{\partial}{\partial \dot{\epsilon}} \langle \mathcal{W} \rangle = A\dot{\epsilon} \tag{35}$$

where

$$N = \begin{bmatrix} N_{11} & N_{22} & N_{12} & M_{11} & M_{22} & M_{12} \end{bmatrix}^{\mathrm{T}} \tag{36}$$

Based on the results of the Euler step, the Newton step proceed. To do so, writing Eq. (27) in an incremental form

$$\delta U^* = \left\langle \Delta\sigma_{ij}\delta\left(\Delta\Gamma_{ij}\right)\right\rangle = 0 \tag{37}$$

discretizing Ep. (37) gives

$$\begin{aligned} \delta U^* &= \langle [\sigma(V) - \sigma_n]\, \delta\, [\Gamma_h S (V - V_n)] \rangle \\ &= \delta V^{\mathrm{T}} \left\langle (\Gamma_h S)^{\mathrm{T}} [\sigma(V) - \sigma_n] \right\rangle \\ &= 0 \end{aligned} \tag{38}$$

where

$$\sigma = \begin{bmatrix} \sigma_{11} & \sigma_{22} & \sigma_{33} & \sigma_{23} & \sigma_{13} & \sigma_{12} \end{bmatrix}^{\mathrm{T}} \tag{39}$$

and the subscript n denotes the value at the beginning of the current increment. Notice here the stress σ is calculated using the nonlinear material model, and generally $\sigma \neq D\Gamma$. Eq. (38) holds only if

$$\Psi(V) = \left\langle (\Gamma_h S)^{\mathrm{T}} [\sigma(V) - \sigma_n] \right\rangle = 0 \tag{40}$$

Suppose the Newton step converged in the previous increment, then

$$\left\langle (\Gamma_h S)^{\mathrm{T}} \sigma_n \right\rangle = 0 \tag{41}$$

As a result,

$$\Psi(V) = \left\langle (\Gamma_h S)^{\mathrm{T}} \sigma(V) \right\rangle = 0 \tag{42}$$

To solve Eq. (42), it requires that

$$\Psi\left(V_{old}+\mathrm{d}V\right)=\Psi\left(V_{old}\right)+\frac{\partial\Psi}{\partial V}\mathrm{d}V=0 \tag{43}$$

where

$$\frac{\partial\Psi}{\partial V}=\left\langle\left(\Gamma_h S\right)^{\mathrm{T}}\frac{\partial\sigma}{\partial V}\right\rangle=\left\langle\left(\Gamma_h S\right)^{\mathrm{T}}D\left(\Gamma_h S\right)\right\rangle=E \tag{44}$$

Then using Eq. (44), the correction can be computed from Eq. (43) and added to the solution, i.e.,

$$V_{new}=V_{old}+\mathrm{d}V \tag{45}$$

The resultant sectional force and moment N can be obtained through differentiating U, which gives

$$\begin{aligned}\dot{N}&=\frac{\partial}{\partial\dot{\epsilon}}\left\langle\mathcal{W}\right\rangle=\left\langle\frac{\partial\mathcal{W}}{\partial\dot{\epsilon}}\right\rangle=\left\langle\left(\frac{\partial\dot{\Gamma}}{\partial\dot{\epsilon}}\right)^{\mathrm{T}}\frac{\partial\mathcal{W}}{\partial\dot{\Gamma}}\right\rangle\\&=\left\langle\left(\Gamma_h S\frac{\partial V}{\partial\epsilon}+\Gamma_\epsilon\right)^{\mathrm{T}}\dot{\sigma}\right\rangle\end{aligned} \tag{46}$$

Because of Eq. (42), the first term in the bracket of Eq. (46) will be zero when multiplied with $\dot{\sigma}$, so that

$$\dot{N}=\left\langle\Gamma_\epsilon^{\mathrm{T}}\dot{\sigma}\right\rangle \tag{47}$$

then

$$N=\int_0^t\dot{N}\mathrm{d}t=\left\langle\Gamma_\epsilon^{\mathrm{T}}\sigma\right\rangle \tag{48}$$

From the expression of the sectional force and moment in Eq. (48), a Jacobian defining the relation between 2D strain and sectional force increments can be obtained as

$$\frac{\partial N}{\partial\epsilon}=\frac{\left\langle\Gamma_\epsilon^{\mathrm{T}}\partial\sigma\right\rangle}{\partial\epsilon}=\left\langle\Gamma_\epsilon^{\mathrm{T}}\frac{\partial\sigma}{\partial\Gamma}\frac{\partial\Gamma}{\partial\epsilon}\right\rangle=\left\langle\Gamma_\epsilon^{\mathrm{T}}D\Gamma_\epsilon\right\rangle=D_{\epsilon\epsilon} \tag{49}$$

Although the above derivation is based on 1D SG, the methodology is general. Not only the classical shell model with 2D or 3D SG, but also beam or micromechanics model can be constructed with appropriate modifications of the kinematics. The shell and micromechanics models were implemented in a modified version of the general-purpose constitutive modeling code SwiftComp.

IV. Nonlinear Analysis with SwiftComp

In this section, details of the nonlinear solving algorithm for SwiftComp are introduced. In nonlinear analysis, effective properties of the structure are dependent on the loading state. As a result, the homogenization needs to be integrated with the structural simulation, with the effective properties updated every iteration of the structural simulation.

In Abaqus, this can be done through the user subroutine UGENS, with the UGENS acting as an interface to call and pass data to the nonlinear SwiftComp, and receive the output from the nonlinear SwiftComp. Fig. 2 shows the procedure of a 2-step nonlinear homogenization, containing a 3D homogenization step representing the lamina/yarn and a shell step representing the laminate/woven composite. At every integration point in the structural simulation,

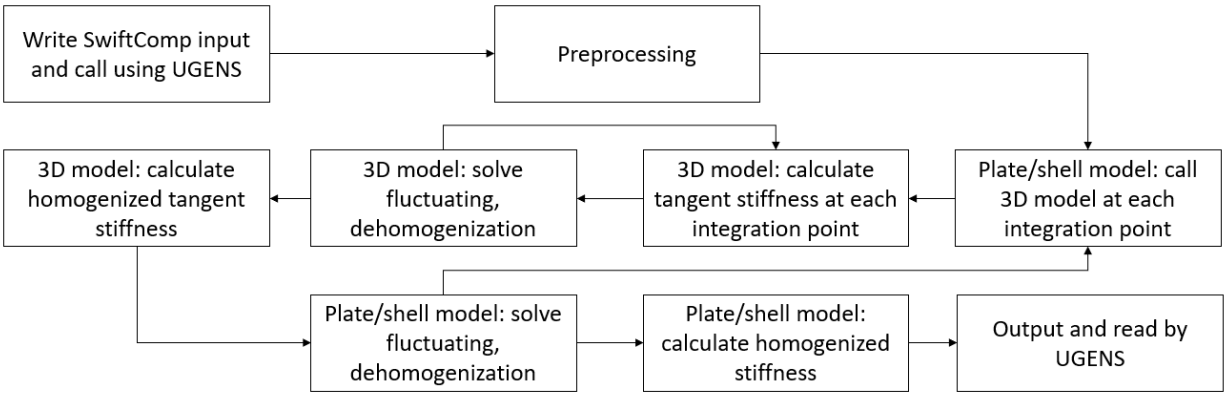

Fig. 2 Procedure of nonlinear homogenization for composites with SwiftComp.

the UGENS can be called and a SwiftComp input file will be generated at the start of every iteration. The nonlinear SwiftComp will read the input and preprocess, and start the shell level homogenization. At each integration point of the shell SG, the process of 3D solid homogenization will be called. In this step of homogenization, the tangent stiffness of the lamina or yarn will be calculated based on the nonlinear material model. This process is done by iterations and loops until the homogenization converges. The resultant 3D tangent stiffness will be used for shell level homogenization, and similarly, the shell level homogenization is also iterated until convergence. If the current iteration is not converged, it will go back to the 3D homogenization step and re-calculate the tangent stiffness based on the updated stress and strain at the integration point of the shell SG. Once the shell homogenization is converged, the tangent ABD stiffness can be output and read by the UGENS for the structural simulation. This paper focuses on the process of calculating the tangent stiffness of an integration point in the structural simulation, i.e., the nonlinear homogenization performed by SwiftComp.

To easily model various nonlinear material behaviors, the user material capability of nonlinear SwiftComp was developed. This capability allows implementing a nonlinear material into a separated subroutine without changing the other part of the SwiftComp code. For the convenience of the user, the user material for SwiftComp, called SCUMAT, was developed to be similar to the Abaqus UMAT user subroutine. The format of the SCUMAT is:

```
      module UserMaterial
      contains
c
      subroutine SCUMAT(stress,statev,ddsdde,
     1 stran,dstran,time,dtime,
     2 ndi,nshr,ntens,nstatv,props,nprops,
     3 noel,npt,kstep,kinc)
c
      integer ndi,nshr,ntens,nstatv,nprops,
     1 noel,npt,kstep,kinc
      double precision stress(ntens),statev(nstatv),
     1 ddsdde(ntens,ntens),stran(ntens),dstran(ntens),
     2 time(2),dtime,props(nprops)
c
c Code for defining the user material
c
      return
      end
      end module UserMaterial
```

Same with the Abaqus UMAT, in SCUMAT, the variables to be defined by the user are: *stress* (the stress at the end of the increment), *statev* (the solution dependent variables (SDVs)), and *ddsdde* (Jacobian matrix of the material model). Other variables are also defined in the same manner as the Abaqus UMAT, and their meaning can be found in the Abaqus documentation [25]. The number of SDVs and user defined material properties can be specified in the SwiftComp input file. The format of SCUMAT and inputs needed for the user material minimize the effort of converting an Abaqus UMAT into an SCUMAT.

V. Numerical Examples

In this section, a few numerical examples to validate the MSG-based nonlinear shell model are presented along with the user material capability of the nonlinear SwiftComp.

A. Viscoelastic Model

Firstly, nonlinear shell analysis without the 3D homogenization step needs to be validated. This can be done by comparing SwiftComp results with Abaqus. To do so, a plate was created in Abaqus using 3D solid elements, with the

geometry and boundary conditions shown in Fig. 3. The 3D solid element is chosen so that the material model in the UMAT can be directly applied to the plate without going through the built-in shell section in Abaqus. The plate is

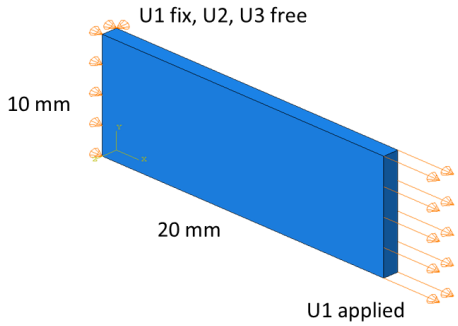

Fig. 3 Plate test sample in Abaqus.

homogeneous and the thickness is 1 mm. By applying a displacement U_1, a normal strain of ϵ_{11} can be generated at the center of the plate, with other strain components being zero. The comparison with the nonlinear SwiftComp shell model can be done by analyzing the stress and strain through the thickness at the center of the plate and obtain the shell strain and curvature ϵ and κ, and the sectional force and moment N and M. The SCUMAT used in the nonlinear SwiftComp is converted from the Abaqus UMAT.

The nonlinear material model is a simple viscoelastic model from the Abaqus UMAT documentation [25]. A diagram of the model is shown in Fig. 4. The stress-strain relation of the model can be generalized as an isotropic solid

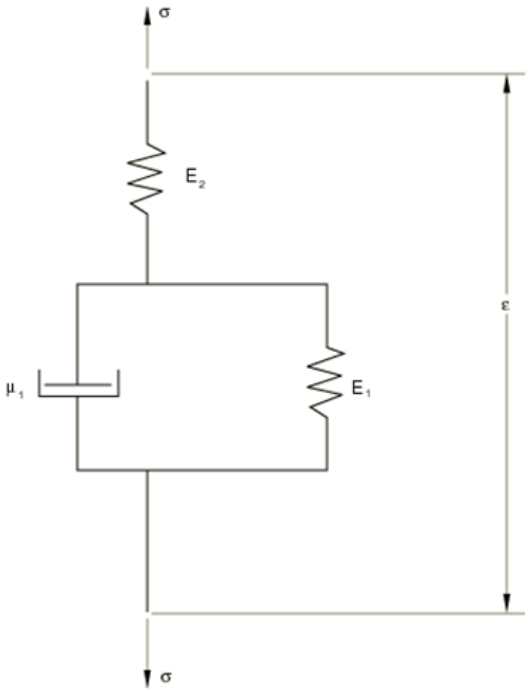

Fig. 4 Diagram of the simple viscoelastic model.

as [25]

$$\sigma_{11} + \bar{\nu}\dot{\sigma}_{11} = \lambda\epsilon_V + 2\mu\epsilon_{11} + \bar{\lambda}\dot{\epsilon}_V + 2\tilde{\mu}\dot{\epsilon}_{11} \tag{50}$$

$$\sigma_{12} + \bar{\nu}\dot{\sigma}_{12} = \mu\epsilon_{12} + \tilde{\mu}\dot{\epsilon}_{12} \tag{51}$$

The model has 5 user defined material properties, with their values used in the analysis shown in Table 1, where λ and μ are Lamé constants, $\bar{\lambda}$, $\tilde{\mu}$ and $\bar{\nu}$ are viscoelastic constants, and $\epsilon_V = \epsilon_{11} + \epsilon_{22} + \epsilon_{33}$. The displacement U_1 is applied to be

Table 1 User defined properties of the simple viscoelastic material.

λ	μ	$\bar{\lambda}$	$\tilde{\mu}$	$\bar{\nu}$
693	195	22587	6496	56

0.2 mm, generating a strain of 1%. Since this is a viscoelastic material model, two loading rates are used, with the loading process finished in 1 s or 100 s. Results are shown in Fig. 5. It can be seen that no matter the loading rate,

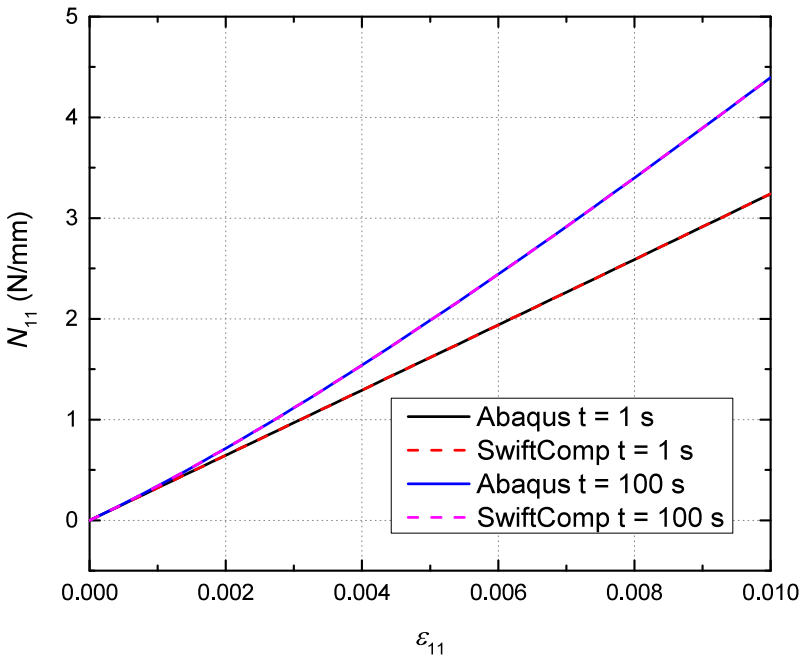

Fig. 5 Loading curve of the simple viscoelastic model.

the curves from nonlinear SwiftComp overlap with the curves from Abaqus, showing the validity of running with a time-dependent user material in nonlinear SwiftComp.

B. Continuum Damage Model

The second example is a continuum damage model, developed by Zhang and Yu [26]. This model is originally developed based on an explicit algorithm, so it is not rigorous to apply it in the implicit nonlinear SwiftComp, but it can still serve for testing purposes. In this model, the update of the stress is given in a rate form:

$$\dot{\boldsymbol{\sigma}} = \left\{ [-(\boldsymbol{\mathscr{F}} : \boldsymbol{\epsilon}) : \mathcal{E} + \boldsymbol{\mathscr{G}} : \boldsymbol{\epsilon}] : \tilde{\mathcal{N}}^{-1} + C^e \right\} : \dot{\boldsymbol{\epsilon}} \tag{52}$$

where C^e is the elastic stiffness tensor before any damage; $\mathcal{E}$ and $\tilde{\mathcal{N}}$ are fourth-order coefficient tensors; $\boldsymbol{\mathscr{F}}$ and $\boldsymbol{\mathscr{G}}$ are sixth-order coefficient tensors. When implemented as SCUMAT, this rate form is used in incremental form, and strain rate and strain at the start of the current iteration, $\boldsymbol{\epsilon}$, are known. All the coefficient tensors can be calculated based on elastic stiffness, strain state, and other damage related parameters. Details of the model can be found in [26]. This model has 12 user defined material constants and 9 SDVs, as shown in Tables 2 and 3. In this example the displacement

Table 2 User defined properties of the damage model.

Material Properties (12)	Value
Isotropic elatic modulus (MPa)	38500
Isotropic Poisson's ratio	0.24
Damage threshold (MPa)	1.6e-5
Damage model parameter 1	0.5
Damage model parameter 2	0.5
Damage surface shape parameter	1
Damage anisotropy vector	(1, 1, 1, 1, 1, 1)

Table 3 SDV of the damage model.

SDV (9)
Current damage threshold
Current damage accumulation variable
Damage variable, 6 components
Element delete flag

applied is 0.024 mm, generating a normal strain of 0.12%. The strain is not further increased because originally the model is developed for explicit analysis and implemented as a VUMAT, and a direct conversion to UMAT makes the model not stable in implicit analysis. Increasing the strain will lead to convergence issues in both Abaqus and nonlinear SwiftComp. The loading curve of the model is shown in Fig. 6. It can be seen from Fig. 6 that nonlinear SwiftComp have an excellent match with Abaqus results. The examples in Section A and B validate that the user material capability of the nonlinear SwiftComp can be used in the same way as the Abaqus UMAT and generates reliable results.

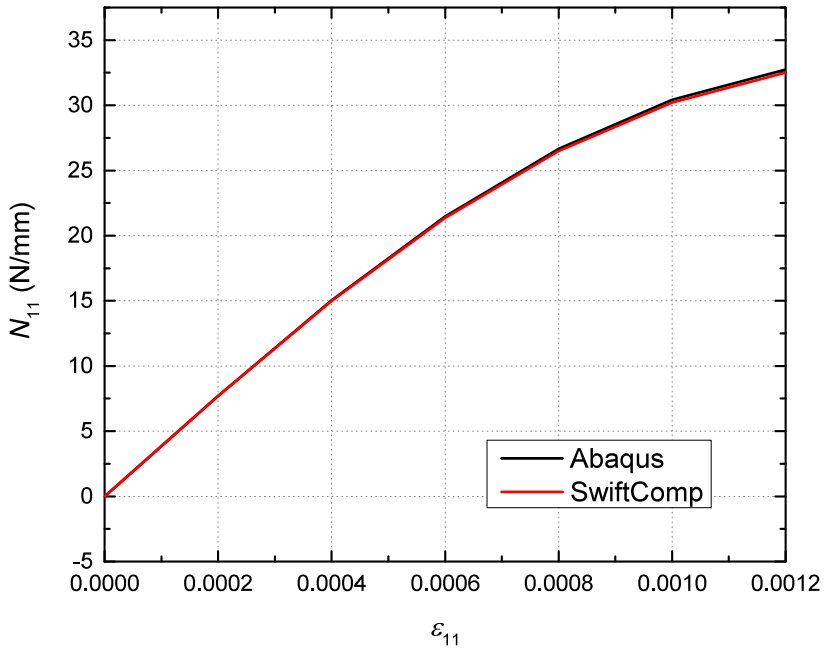

Fig. 6 Loading curve of the damage model.

C. Nonlinear Viscoelastic-Viscoplastic Model

The nonlinear viscoelastic-viscoplastic model used in this section was developed by Zhang [27]. The model consists of two parts: a nonlinear viscoelastic part that governs the resin behavior before yielding, and a viscoplastic part that calculates the permanent deformation. In the viscoelastic part, the tangent stiffness $\tilde{C}$ and stress increment $\Delta\boldsymbol{\sigma}$ can be calculated with:

$$\tilde{C}^{-1} = \tilde{J}\mathcal{I}' + \frac{1}{3}\tilde{B}\boldsymbol{I}\otimes\boldsymbol{I} \tag{53}$$

$$\Delta\boldsymbol{\sigma} = \tilde{C} : \Delta\boldsymbol{\epsilon} + \sum_{i=1}^{N}\left[1-\exp\left(-\lambda_i\Delta\psi\right)\right]\tilde{C} : \left(\boldsymbol{\epsilon}_i\right)_n \tag{54}$$

where $\tilde{J}$ and $\tilde{B}$ are scalars calculated from the shear and the bulk compliance, along with stress-dependent functions and stress-dependent effective time ψ; $\mathcal{I}'$ is the deviatoric part of the fourth-order identity tensor; $\boldsymbol{I}$ is the second-order identity tensor; λ_i are the inverse of relaxation time; $\boldsymbol{\epsilon}_i$ are strain components decomposed based on the 1D generalized Maxwell model. When the resin starts yielding, viscoplastic deformation happens. In this case, a radial return algorithm is used and the stress can be updated with:

$$\boldsymbol{\sigma} = \beta + \boldsymbol{\sigma} \tag{55}$$

And the tangent operator C^{alg} can be calculated with:

$$C^{alg} = \left(\mathcal{I} + \frac{\partial \boldsymbol{X}}{\partial \beta} - \frac{\frac{\partial \boldsymbol{X}}{\partial \Delta v} \otimes \frac{\partial \mathrm{P}}{\partial \beta}}{\frac{\partial \mathrm{P}}{\partial \Delta v}} \right) : \left(\frac{\partial \boldsymbol{\Psi}}{\partial \beta} - \frac{\frac{\partial \boldsymbol{\Psi}}{\partial \Delta v} \otimes \frac{\partial \mathrm{P}}{\partial \beta}}{\frac{\partial \mathrm{P}}{\partial \Delta v}} \right)^{-1} : \tilde{C} \tag{56}$$

where $\boldsymbol{X}$ is the back stress tenor due to kinematic hardening; β is a stress related tensor to be updated in the algorithm; v is a viscoplastic multiplier; $\mathrm{P} = \Delta v - \dot{v}\Delta t$; $\boldsymbol{\Psi}$ is another stress related tensor. Details of this constitutive model can be found in [27].

Firstly, the nonlinear viscoelastic part of the constitutive model introduced is implemented into SCUMAT and tested with the nonlinear SwiftComp. For comparison, experimental data of polymethyl methacrylate (PMMA) from Lai and Bakker [28] is used. The material model has eleven user-defined material constants, ten of them being the Prony series

Table 4 Viscoelastic parameters of the PMMA material in terms of a Prony series [28].

n	λ_n (s^{-1})	$D_n \times 10^{-6}$ (MPa^{-1})
1	1	23.6358
2	10^{-1}	5.6602
3	10^{-2}	14.8405
4	10^{-3}	18.8848
5	10^{-4}	28.5848
6	10^{-5}	40.0569
7	10^{-6}	60.4235
8	10^{-7}	79.6477
9	10^{-8}	162.1790
D_0		270.9000

expressed in terms of compliance, D_n, as shown in Table 4, and the last one being the Poisson's ratio $\nu = 0.39$. In order to show the capability of the nonlinear SwiftComp on shell modeling, a shell model is used instead of a solid model. For a straightforward comparison, the thickness of the shell is 1 mm. In the analysis, the shell is loaded with a tensile sectional force of 30 N/mm instantaneously, and kept for 1800 s for creep. After that, the load is reduced to 25 N/mm, and kept for another 1800 s for creep recovery. Results are shown in Fig. 7. We can see that the strain has an excellent match during the creep, while underestimation exists during the creep recovery period, with an error of about 4%. A possible cause of underestimation can be that plastic deformation already happened in the experiment during the creep step while it is not included in the numerical model. Responses of the model under different load magnitudes are also compared. In the experiments [28], the specimens are loaded in tension with 15, 20, 25, and 30 MPa respectively. Using the same 1 mm thick shell geometry, prescribed section forces of 15, 20, 25 and 30 N/mm are applied in the nonlinear SwiftComp model. After the creep time of 1800 s, the load is completely removed and the specimen is allowed to recovery for 1800 s. The resultant strains during creep are shown in Fig. 8 and during recovery in Fig. 9. In these two figures, different line types are used to represent different load magnitudes, with the unit of MPa

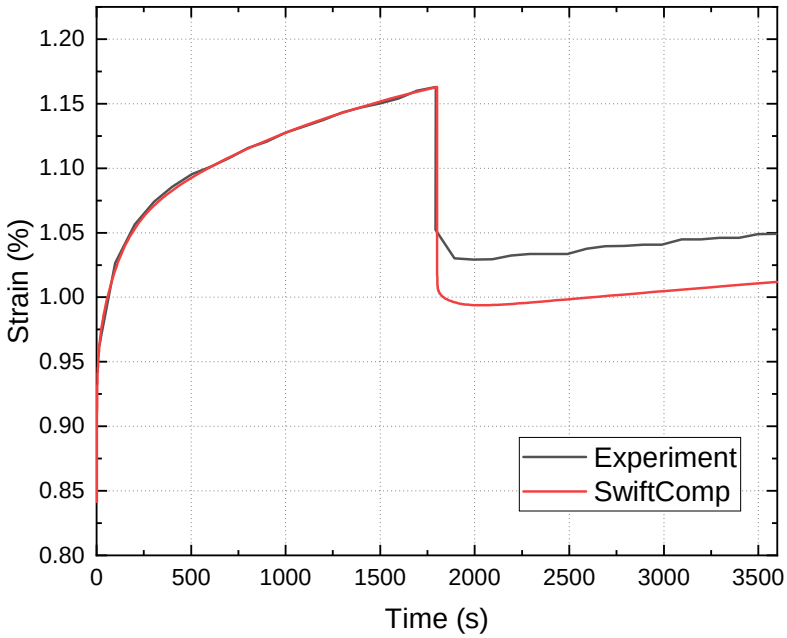

Fig. 7 Strain history of a nonlinear viscoelastic shell under creep and creep recovery.

for experimental results plotted in black, or the equivalent N/mm for the SwiftComp results plotted in red. Similar to the previous example, the nonlinear SwiftComp model provides excellent matches for the creep and some deviation can be observed during the recovery. The deviation increases with magnitude of the load.

Another example is studied with the constitutive model using a hexagonal pack as a 2D SG for 3D solid homogenization, as shown in Fig. 12. The capability of 3D solid homogenization needs to be validated as it is necessary in the 2-step homogenization. The nonlinear viscoelastic material model is used for the resin matrix and the fiber is elastic, with the properties shown in Table 5. A tensile load is applied incrementally over 180 seconds in the fiber direction to produce a final 1% strain. Then the strain is kept for 1800 seconds for relaxation. The stress history of the loading process is shown in Fig. 10. Due to the load being applied in the fiber direction, the curve looks bi-linear, and the stress magnitude is large compared with previous examples with the homogeneous material. However, when focusing on the relaxation part, as shown in Fig. 11, the stress relaxation can be observed. This shows the capability of the nonlinear SwiftComp and the SCUMAT to capture the nonlinear viscoelastic behavior for both shell and 3D solid models.

To analyze the material behavior after yielding, the viscoplastic part of the constitutive model is also implemented in a SCUMAT. This model has a total of eighteen user-defined material constants. The viscoelastic part uses the same Prony series and Poisson's ratio as the previous model shown in Table 4. Seven viscoplasticity related material constants are shown in Table 6, where σ_y is the initial yield stress; Q and b are isotropic hardening parameters; C and a are

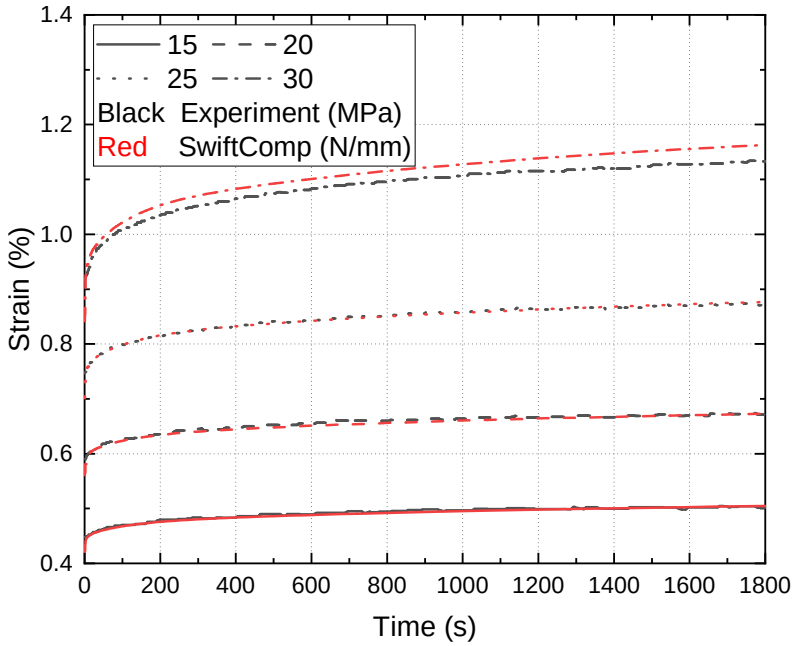

Fig. 8 Strain history of a nonlinear viscoelastic shell under different load magnitude during creep.

kinematic hardening parameters; γ is a viscosity parameter; n is a rate-sensitivity parameter. The model is tested with a homogeneous shell model with a thickness of 0.2 mm. The loading history consists of four steps: loading, relaxation, unloading, and recovery. The shell is loaded under pure bending with an axial curvature of 0.18 mm^{-1} over 100 s. Two relaxation times are compared, 9000 s and 18000 s. Then the shell is unloaded to a moment-free state over 100 s, and followed by the recovery over 36000 s. The moment-curvature graph during the loading cycle is shown in Fig. 13. During relaxation, the moment diminishes while the curvature remains the same, and longer relaxation times result in a bigger reduction. Although the loading and unloading curves look linear, after recovery, residual curvature can be

Table 5 Engineering constants of the fiber.

E_1 (MPa)	2.94×10^5
E_2 (MPa)	2.91×10^4
E_3 (MPa)	2.91×10^4
ν_{23}	0.20
ν_{13}	0.20
ν_{12}	0.46
G_{23} (MPa)	1.13×10^4
G_{13} (MPa)	1.13×10^4
G_{12} (MPa)	1.00×10^4

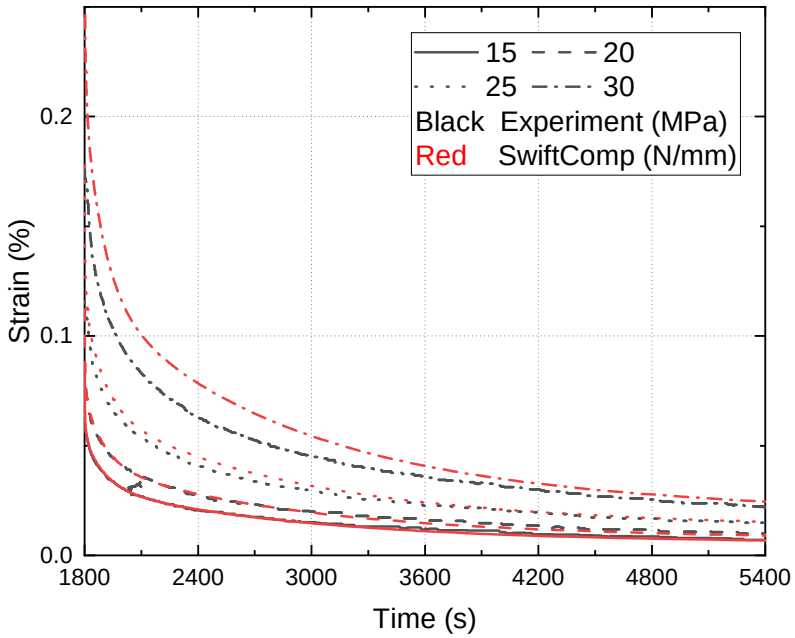

Fig. 9 Strain history of a nonlinear viscoelastic shell under different load magnitude during recovery.

observed in both cases, as shown in Fig. 14. At the end of the recovery. the residual curvature of the 18000-second relaxation time case is 32.6% larger than the 9000-second case, even though their loaded curvatures are the same. This means that in both cases the material has yielded, and the plastic deformation happens to be accumulating during the relaxation step, demonstrating that the developed models can capture viscoplastic behavior.

D. 2-Step Homogenization

For some structures such as laminates or woven composites shells, a 2-step homogenization with a 3D solid step and a shell homogenization step is necessary. The 2-step homogenization shown in Fig. 2 is tested with the nonlinear

Table 6 Viscoplastic material parameters.

Parameter	Value
σ_y (MPa)	35
Q (MPa)	5.50879
b	53.2535
C (MPa)	1035.167
a	140.2
γ (s^{-1})	1.00845×10^{-4}
n	8.27066

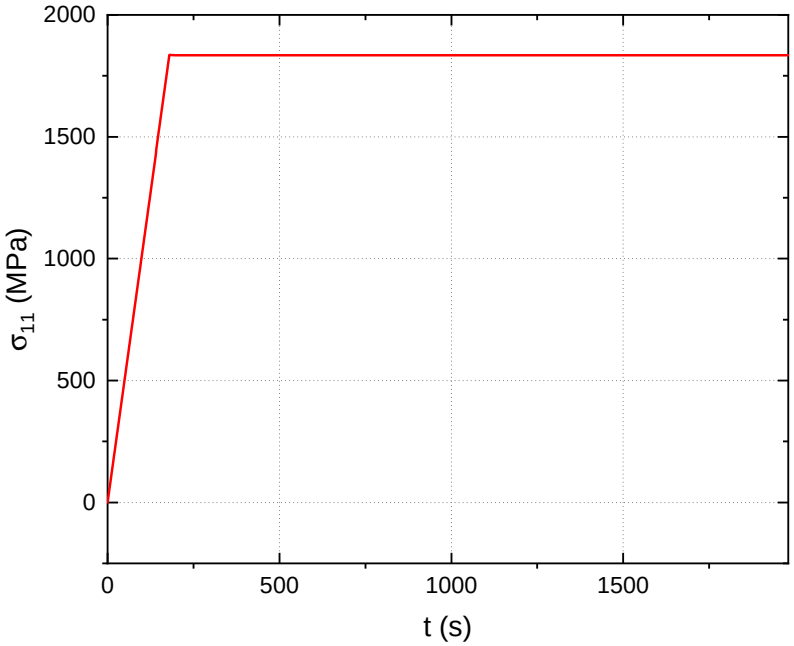

Fig. 10 Stress history of the hexagonal pack.

SwiftComp. The SG used in the 3D solid step is shown in Fig. 12, a hexagonal pack consisting of fibers and the matrix that represents the lamina. The matrix uses the viscoelastic model from Abaqus presented in Section A, and the fiber is elastic, with the material properties shown in Table 5. The shell model uses a 1D SG, with one element representing a one-layered shell. The thickness of the shell is 1 mm. In order to better observe the behavior caused by the viscoelastic material model of the matrix, bending in the normal direction to the fiber is applied. A curvature of 0.02 mm^{-1} is applied with two curvature rates, resulting in a loading time of 1 s and 100 s respectively. The moment-curvature graphs are shown in Fig. 15. It can be seen that with a slower loading speed, the shell generates more moment, and the curve is more nonlinear. As expected, the behavior of the matrix material in the 3D solid step is reflected in the behavior of the shell model. However, the 2-step homogenization has the drawback of being computational expensive. Both loading cases take about 6 hours to run with an Intel(R) Xeon(R) E5-2697 CPU on a server, and the cost will be greatly increased if the shell model uses a more complex SG, such as a 3D SG representing a woven composite. This makes applying the method to structural analysis impractical. A possible solution to this is to construct a surrogate model based on the results of the nonlinear homogenization. For example, a surrogate model can be constructed to represent the behavior of the lamina, substituting the 3D solid step, and then the 2-step homogenization approach can be avoided by using the surrogate model in the shell homogenization step.

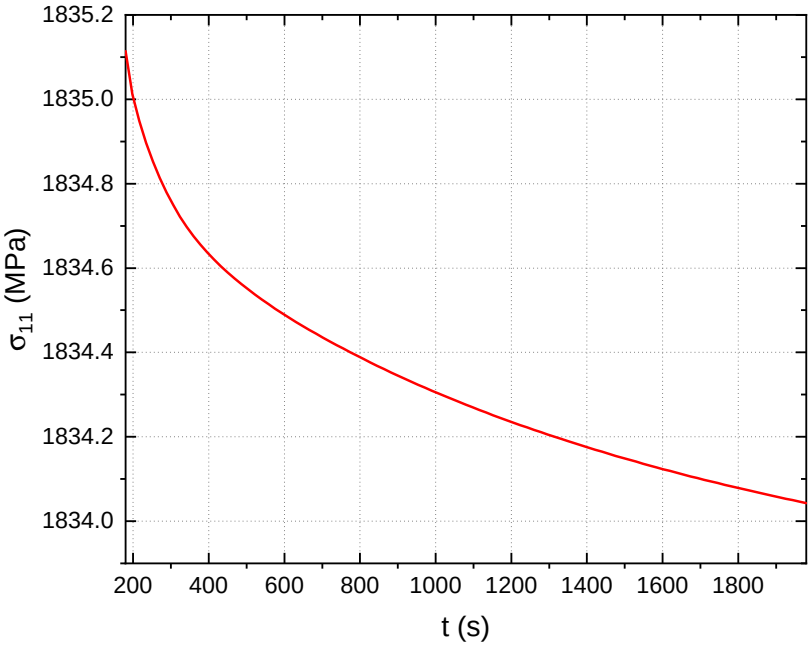

Fig. 11 Stress history of the hexagonal pack during relaxation.

E. Nonlinear SwiftComp with Surrogate Model

In this preliminary study of the surrogate model, the original behavior of the SG is fitted into a polynomial as the surrogate model. For simplicity, the 2D SG in Fig. 12 is used, as well as the same viscoelastic resin and elastic fiber shown in Tables 1 and 5. The polynomial surrogate model is generated using Dakota [29]. It uses a quadratic function in the form of:

$$f(\mathbf{x}) = c_0 + \sum_{i=1}^{n} c_i x_1 + \sum_{i=1}^{n} \sum_{j \geqslant i}^{n} c_{ij} x_i x_j \tag{57}$$

Fig. 12 2D SG of the fiber reinforced composite.

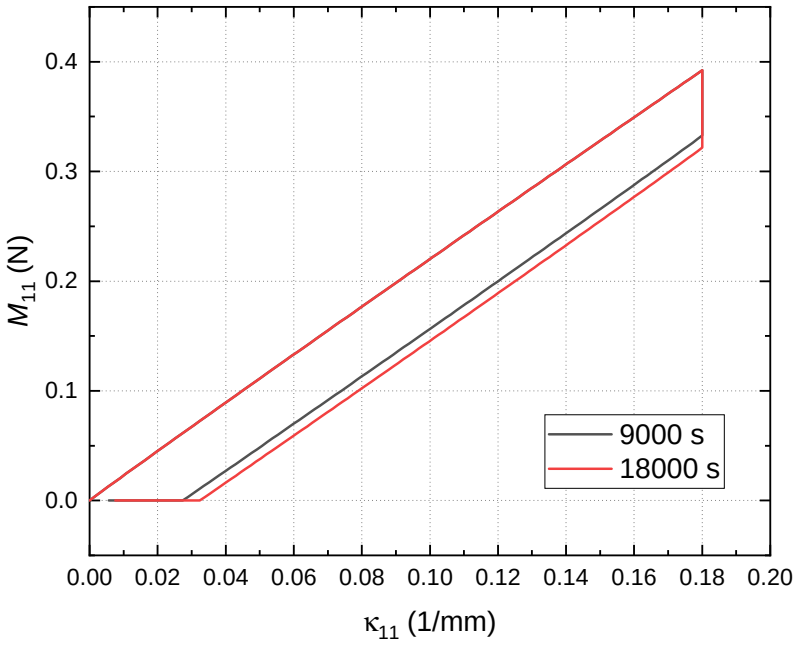

Fig. 13 Moment-curvature curve of the viscoelastic-viscoplastic shell.

where $f(\mathbf{x})$ represents each response of the surrogate model; x_i are terms of the design parameters vector $\mathbf{x}$; n is the dimension of $\mathbf{x}$; and c_0, c_i and c_{ij} are the coefficients of the polynomial to be fitted by data. Due to the material properties and the geometry of the SG, there is no coupling between normal and shear behavior. As a result, when investigating the normal behavior of the SG, the design parameters only need to include the normal terms of the macro strains ϵ_{11}, ϵ_{22} and ϵ_{33}. The model consists of 24 responses, representing the 3 normal terms of the macro stresses and 21 terms in the 3D effective stiffness matrix. The coefficients of the polynomials are determined based on the sample data provided to Dakota. In this study, the sample data are generated through nonlinear 3D homogenization of the SG. Since this is a preliminary study, separate surrogate models are constructed for different loading cases and these surrogate models are not for general purpose.

The surrogate model constructed for 3D homogenization of the 2D SG is implemented in another SCUMAT as if is a homogenized material, and this SCUMAT substitutes the 3D solid homogenization step in the 2-step homogenization. In the following example, a tensile strain of 1% is applied on a single-layer shell model, represented by a 1D SG, in the normal direction to the fiber. To generate the sample data for surrogate modeling, the 2D SG is applied with a tensile strain of 1.5% in the normal direction to the fiber. A larger strain is used in the surrogate modeling for the purpose of avoiding extrapolation of the data. The results of the shell analysis with the surrogate model is compared with the 2-step homogenization with the same parameters, in Fig. 16. It can be seen that the surrogate model matches closely to the

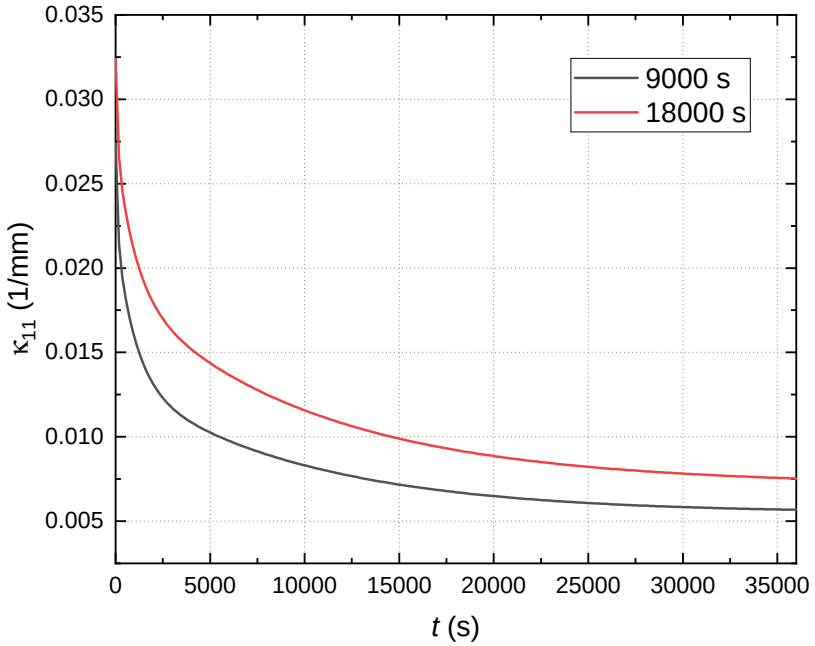

Fig. 14 Residual curvature of the viscoelastic-viscoplastic shell during recovery.

2-step homogenization model. Overestimation exist when the strain goes higher, with an maximum error of 4.3%. the computational cost of the analysis with surrogate models is determined by the sample data generation, surrogate model constructioin, and the shell homogenization step. In this example, compared to the computational time of approximately 6 hours for the 2-step homogenization, the sample data generation and surrogate model construction together take about 1 hour and the shell homogenization step takes less than 1 minute. On the other hand, during the study it was also found that surrogate models were highly sensitive to the sample data. If the strain state passed to the surrogate model is far from that of the sample data, significant loss of accuracy or divergence can happen. Therefore, to construct a more general-purpose surrogate model, large amount of sample data generated with different loading conditions is necessary.

VI. Conclusions

In this paper, a nonlinear shell theory is developed based on the mechanics of structure genome (MSG). With the kinematics capable of handling geometric nonlinearity, the nonlinear shell theory adopts a combined Euler-Newton method, with a Euler step implemented first to initiate the loading in the tangent direction, and then a Newton step used to calculate the correction to obtain a converged solution.

The nonlinear shell model is implemented in a nonlinear version of SwiftComp, and a 2-step homogenization strategy that can link the MSG-based nonlinear shell analysis with the global structural analysis using Abaqus is proposed. With

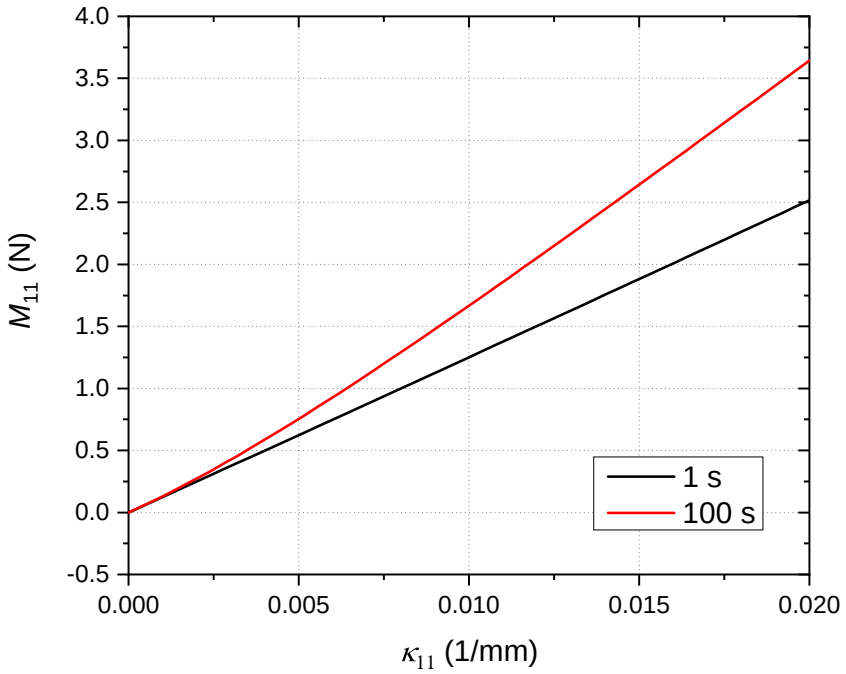

Fig. 15 Moment-curvature curves of the 2-step homogenization.

the 2-step homogenization, analysis of laminates and woven composites are made possible by a 3D homogenization step for the lamina/yarn and a shell modeling step for the laminate/woven composites. For the convenience of implementing different types of nonlinear material constitutive models, a user-material interface called SCUMAT that shares similarity with Abaqus UMAT is developed.

Validation of the nonlinear SwiftComp is done by comparing results with Abaqus models. A simple viscoelastic material and a continuum damage model are tested and both show excellent match with the Abaqus results. In addition, by comparing with experiments in literature, a nonlinear viscoelastic-viscoplastic model is also tested. Nonlinear SwiftComp results match well during creep, while 4% of error is observed during recovery. A 3D homogenization with the nonlinear viscoelastic resin and elastic fiber is demonstrated. Permanent deformation caused by different relaxation time is also analyzed, with a longer relaxation time generating more plastic deformation under the same prescribed curvature. The 2-step homogenization approach using nonlinear SwiftComp is demonstrated with a unidirectional fiber reinforced composite shell, but it results in high computational cost. To reduce the high computational cost of 2-step nonlinear homogenization, a preliminary study on using surrogate models to substitute the 3D solid homogenization step of the 2-step homogenization is carried out. Results show that the surrogate model can produce similar results compared to the 2-step homogenization, with an error less than 5%, while greatly reducing the computational time, from 6 hours of the 2-step homogenization to 1 hour with surrogate model including the sample data generation time.

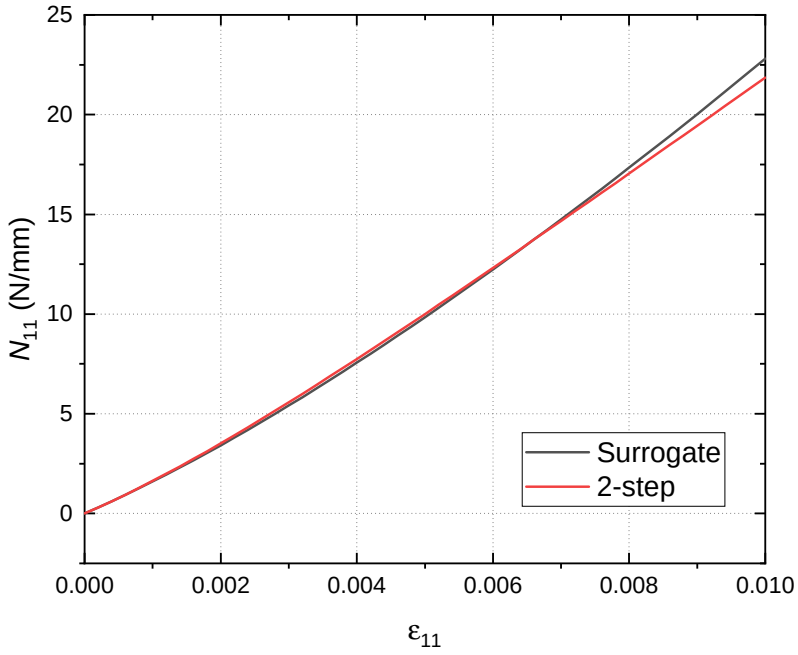

Fig. 16 Force-strain curve of the shell with a surrogate model and 2-step homogenization.

In the future, a machine-learning-based general-purpose surrogate model can be constructed so that the computational cost of the nonlinear MSG-based multiscale modeling approach can be practical for real applications.

Funding Sources and Acknowledgments

This research was partially supported by the NASA Small Business Technology Transfer (STTR) program's Phase I project T12.01-5412 with contract number 80NSSC20C0583. Also by the Space Act Agreement SAA-29213, Annex 2, between Purdue University and NASA LaRC. The views and conclusions obtained herein are those of the authors and should not be interpreted as necessarily representing the official policies or endorsement, either expressed or implied of the funding agency.

References

[1] Adams, D. S., and Mobrem, M., "Lenticular jointed antenna deployment anomaly and resolution onboard the Mars Express spacecraft," *Journal of Spacecraft and Rockets*, Vol. 46, No. 2, 2009, pp. 403–410.

[2] Keil, T., and Banik, J., "Stowage and deployment strength of a rollable composite shell reflector," *52nd AIAA/ASME/ASCE/AHS/ASC Structures, Structural Dynamics and Materials Conference 19th AIAA/ASME/AHS Adaptive Structures Conference 13t*, 2011, p. 2103.

[3] Fernandez, J., Banik, J., and Ardelean, E., "Creep effects and deployment characterization of rollable composite shell reflectors," *53rd AIAA/ASME/ASCE/AHS/ASC Structures, Structural Dynamics and Materials Conference 20th AIAA/ASME/AHS Adaptive Structures Conference 14th AIAA*, Honolulu, Hawaii, 2012.

[4] Ramm, E., and Matzenmiller, A., "Consistent linearization in elasto-plastic shell analysis," *Engineering Computations*, 1988.

[5] Swaddiwudhipong, S., and Liu, Z., "Dynamic response of large strain elasto-plastic plate and shell structures," *Thin-Walled Structures*, Vol. 26, No. 4, 1996, pp. 223–239.

[6] Wang, C., Sun, C., and Gates, T., "Elastic/viscoplastic behavior of fiber-reinforced thermoplastic composites," *Journal of reinforced plastics and composites*, Vol. 15, No. 4, 1996, pp. 360–377.

[7] Peng, X., and Cao, J., "A dual homogenization and finite element approach for material characterization of textile composites," *Composites Part B: Engineering*, Vol. 33, No. 1, 2002, pp. 45–56.

[8] Chen, Y.-C., Rajagopal, K. R., and Wheeler, L., "Homogenization and global responses of inhomogeneous spherical nonlinear elastic shells," *Journal of Elasticity*, Vol. 82, No. 3, 2006, pp. 193–214.

[9] Rabczuk, T., Areias, P. M. A., and Belytschko, T., "A meshfree thin shell method for non-linear dynamic fracture," *International journal for numerical methods in engineering*, Vol. 72, No. 5, 2007, pp. 524–548.

[10] Caseiro, J., Valente, R., Reali, A., Kiendl, J., Auricchio, F., and de Sousa, R. A., "Assumed natural strain NURBS-based solid-shell element for the analysis of large deformation elasto-plastic thin-shell structures," *Computer Methods in Applied Mechanics and Engineering*, Vol. 284, 2015, pp. 861–880.

[11] Goncalves, B. R., Jelovica, J., and Romanoff, J., "A homogenization method for geometric nonlinear analysis of sandwich structures with initial imperfections," *International Journal of Solids and Structures*, Vol. 87, 2016, pp. 194–205.

[12] Yu, W., "A unified theory for constitutive modeling of composites," *Journal of Mechanics of Materials and Structures*, Vol. 11, No. 4, 2016, pp. 379–411.

[13] Yu, W., "Simplified Formulation of Mechanics of Structure Genome," *AIAA Journal*, 2019, pp. 1–9.

[14] Liu, X., Tang, T., Yu, W., and Pipes, R. B., "Multiscale modeling of viscoelastic behaviors of textile composites," *International Journal of Engineering Science*, Vol. 130, 2018, pp. 175–186.

[15] Deo, A., and Yu, W., "Equivalent plate properties of composite corrugated structures using mechanics of structure genome," *International Journal of Solids and Structures*, Vol. 208-209, 2021, pp. 262–271.

[16] Long, Y., Rique, O., Yu, W., Fernandez, J. M., and Bergan, A. C., "Multiscale simulation of deployable composite structures," *AIAA SciTech 2021 Forum*, American Institute of Aeronautics and Astronautics, Virtual Event, 2021. doi:10.2514/6.2021-0199.

[17] Berdichevskii, V. L., "Variational-asymptotic method of constructing a theory of shells: PMM vol. 43, no. 4, 1979, pp. 664–687," *Journal of Applied Mathematics and Mechanics*, Vol. 43, No. 4, 1979, pp. 711–736.

[18] Jiang, F., and Yu, W., "Nonlinear Variational Asymptotic Sectional Analysis of Hyperelastic Beams," *AIAA Journal*, Vol. 54, No. 2, 2016, pp. 679–690.

[19] Jiang, F., and Yu, W., "Damage Analysis by Physically Nonlinear Composite Beam Theory," *Composite Structures*, Vol. 182, 2017, pp. 652–665.

[20] Zhang, L., and Yu, W., "Variational Asymptotic Homogenization of Elastoplastic Composites," *Composite Structures*, Vol. 133, 2015, pp. 947–958.

[21] Zhang, L., Sertse, H. M., and Yu, W., "Variational asymptotic homogenization of finitely deformed heterogeneous elastomers," *Composite Structures*, Vol. 216, 2019, pp. 379–391.

[22] Bensoussan, A., Lions, J.-L., and Papanicolaou, G., *Asymptotic analysis for periodic structures*, Vol. 374, American Mathematical Soc., 2011.

[23] Yu, W., Hodges, D. H., and Volovoi, V. V., "Asymptotic generalization of Reissner–Mindlin theory: accurate three-dimensional recovery for composite shells," *Computer Methods in Applied Mechanics and Engineering*, Vol. 191, No. 44, 2002, pp. 5087–5109.

[24] Yu, W., and Hodges, D. H., "A geometrically nonlinear shear deformation theory for composite shells," *Journal of Applied Mechanics*, Vol. 71, No. 1, 2004, pp. 1–9.

[25] Abaqus, *2017 Documentation*, Dassault Systèmes Simulia Corporation, 2017.

[26] Zhang, L., and Yu, W., "Constitutive modeling of damageable brittle and quasi-brittle materials," *International Journal of Solids and Structures*, Vol. 117, 2017, pp. 80–90.

[27] Zhang, L., Klimm, W., Kwok, K., Fernandez, J. M., Bergan, A. C., and Yu, W., "A Nonlinear Viscoelastic-Viscoplastic Constitutive Model for Epoxy Polymers," *AIAA SciTech 2022 Forum*, American Institute of Aeronautics and Astronautics, San Diego, California, 2022.

[28] Lai, J., and Bakker, A., "3-D Schapery representation for non-linear viscoelasticity and finite element implementation," *Computational mechanics*, Vol. 18, No. 3, 1996, pp. 182–191.

[29] *Dakota, A Multilevel Parallel Object-Oriented Framework for Design Optimization, Parameter Estimation, Uncertainty Quantification, and Sensitivity Analysis: Version 6.11 User's Manual*, Sandia National Laboratories, 2019.